Protein Science (1998), 7:1603–1611. Cambridge University Press. Printed in the USA.

Porin mutants with new channel properties

BENEDIKT SCHMID, LAURENT MAVEYRAUD, MARKUS KRÖMER, AND GEORG E. SCHULZ
Institut für Organische Chemie und Biochemie, Albert-Ludwigs-Universität, Freiburg im Breisgau, Germany

(RECEIVED February 23, 1998; ACCEPTED May 1, 1998)

Abstract

The general diffusion porin from *Rhodopseudomonas blastica* was produced in large amounts in *Escherichia coli* inclusion bodies and (re)natured to the exact native structure. Here, we report on 13 mutants at the pore eyelet giving rise to new diffusion properties as measured in planar lipid bilayer experiments. The crystal structures of seven of these mutants were established. The effects of charge-modifying mutations at the pore eyelet are consistent with the known selectivity for cations. Deletions of 16 and 27 residues of the constriction loop L3 resulted in labile trimers and pores. The reduction of the eyelet cross section by introducing tryptophans gave rise to a closely correlated decrease of the conductivities. A mutant with six newly introduced tryptophans in the eyelet closed its pore in a defined manner within seconds under a voltage of 20 mV, suggesting the existence of two states. The results indicate that the pore can be engineered in a rational manner.

Keywords: lipid bilayer experiments; membrane channel; pore eyelet mutants; *Rhodopseudomonas blastica*; voltage gating; X-ray structure analysis

General diffusion porins are water-filled passive channels spanning the outer membrane of Gram-negative bacteria. They are permeable for small polar solutes with exclusion limits around 600 Da, but exclude nonpolar molecules of comparable sizes. Porins are particularly stable toward heat, detergents, and proteases. Usually porins are found as homotrimeric proteins with molecular masses ranging from 30 to 50 kDa per subunit (Benz & Bauer, 1988; Nikaido, 1994; Schulz, 1996). An initial structure analysis of the major porin from *Rhodobacter capsulatus* demonstrated that the pore of each subunit is formed by a 16-stranded β-barrel constricted to an eyelet near its center (Weiss et al., 1990). The constricting loop L3 contains around 40 residues connecting the fifth with the sixth strand of the β-barrel. The same applies for other general diffusion porins (Schulz, 1993), among them the major porin from *Rhodopseudomonas blastica* (Kreusch et al., 1994; Kreusch & Schulz, 1994), which is the object of the reported investigation (Fig. 1).

Previously reported porin modifications can be subdivided into chemical labeling (Przybylski et al., 1996), growth-selected mutations, for example, for colicin resistance (Jeanteur et al., 1994) or for maltodextrin usage (Benson et al., 1988; Misra & Benson, 1988; Rocque & McGroarty, 1990; Lou et al., 1996; Saint et al., 1996a), and site-directed mutations (Bauer et al., 1989; Bishop et al., 1996; Le Dain et al., 1996; Saint et al., 1996b; Gokce et al., 1997; Srikumar et al., 1997; Van Gelder et al., 1997). As a general result, point mutations altering the charge at the pore eyelet gave rise to ion conductivity and selectivity changes, while growth selection for maltodextrin usage resulted among others in deletions within the constriction loop L3, presumably giving rise to larger eyelet cross sections. Here, we report on the properties and structures of site-directed point mutations as well as deletions in the constriction loop L3 that were meant to alter the charge pattern at the eyelet and to increase or decrease its cross section.

Results and discussion

Because the recombinant porin from *R. blastica* can be produced in inclusion bodies and (re)natured in large amounts to conformationally authentic porin (Schmid et al., 1996), it provides a most suitable system for membrane channel engineering. In our work we followed two lines: first, we changed the charge pattern that causes a transversal electric field across the pore eyelet, proposed to separate polar from nonpolar solutes (Schulz, 1993). In a second series, we changed the cross section of the eyelet. On one hand, we tried to increase it by deleting parts of the constriction loop L3, and on the other, we decreased it by filling the pore eyelet with tryptophans (Fig. 1). In all cases, we kept the exchange E1M of the N-terminal residue introduced for stabilizing the recombinant porin (Schmid et al., 1996).

The stability of the resulting porin was checked by its behavior in SDS polyacrylamide gel electrophoresis (PAGE). A further sta-

Reprint requests to: Dr. Georg E. Schulz, Institut für Organische Chemie und Biochemie, Albertstr. 21, D-79104 Freiburg im Breisgau, Germany; e-mail: schulz@bio5.chemie.uni-freiburg.de.

Abbreviations: C_8E_4, n-octyltetraoxyethylene; Del89-115, Del100-115, mutants in which the respective chain segment is deleted; LDAO, *N,N*-dimethyldodecyl-amine-*N*-oxide; RMSD, root-mean-square deviation; SDS PAGE, sodium dodecylsulfate polyacrylamide gel electrophoresis; 50/52/97/99→A, 96/119→W mutants in which the residues at the stated positions were changed to alanines or tryptophans, respectively.

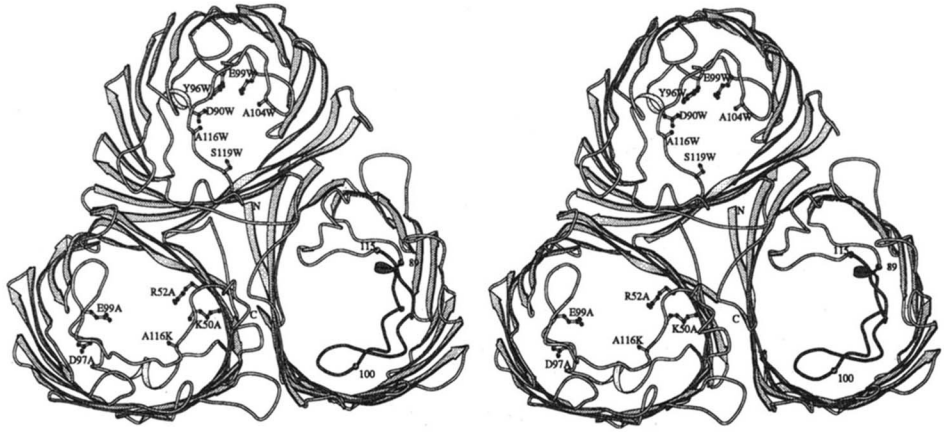

Fig. 1. Stereo view of homotrimeric porin from *R. blastica* with β-strands and a short α-helix depicted as ribbons. The view is from the external medium approximately along the molecular threefold axis, which is perpendicular to the membrane plane. Each chain consists of 289 amino acid residues forming a 16-stranded anti-parallel all-next-neighbor β-pleated sheet (Kreusch et al., 1994). The N- and C-termini are labeled for one subunit. The mutated residues in the charge-modification series (left-hand side), in the tryptophan-introducing series (top), and the border residues for the deletions in the constriction loop L3 (right-hand side) are depicted.

bility indicator is the amount of produced functional recombinant protein and its ability to crystallize (Table 1). Because all mutations were at the inner surface of the pore far away from the crystal contacts, all stable mutants should crystallize like the recombinant and the wild-type porin. This expectation was fulfilled by seven mutants, the structures of which were determined.

Mutations

Mutants A116K, K50A/R52A, D97A/E99A, and the combined four-point mutant 50/52/97/99→A were constructed to disturb the transversal electric field (Figs. 1, 2). For changing the cross section of the eyelet, we produced the deletion mutants Del89-115 and

Table 1. *Stabilities and channel conductances of wild-type and engineered porins*

	Protein[a] (mg)	SDS PAGE[b]	Crystals[c]	Conductance[d] (nS)	Relative conductance (%)	Relative cross section[e] (%)
Wild-type porin	—	t	X-grade	3.9 (0.17)	100	100
Recombinant porin	24	t	X-grade	3.9 (0.17)	100	100
A116K	13	t	X-grade	3.2 (0.19)	82	73
K50A/R52A	27	t	X-grade	4.2 (0.19)	108	107
D97A/E99A	25	t	X-grade	3.7 (0.28)	95	111
50/52/97/99→A	15	t	X-grade	3.9 (0.18)	100	117
Del89–115	7	m	Micro	2.5 (broad)	64	—
Del100–115	5	m	Micro	2.4 (broad)	62	—
104→W	18	t	X-grade	3.5 (0.30)	90	96
96/119→W	17	t	X-grade	3.0 (0.29)	77	78
99/116→W	12	t	X-grade	2.1 (0.30)	54	45
90/99/116→W	2.0	t	nd	2.1 (broad)	54	—
99/116/119→W	1.8	t	nd	1.7 (broad)	44	—
96/104/116/119→W	1.2	t	nd	2.4 (0.55)	62	—
90/96/99/104/116/119→W	0.7	m,t	Micro	2.7 (0.25)	69	22[f]

[a]Total amount of folded protein obtained per liter culture, reflecting expression rates, stabilities, and folding efficiencies.

[b]Migration in SDS PAGE without boiling: m, monomeric; t, trimeric.

[c]The crystallization resulted in an X-ray analysis (X-grade), in crystals that could not be analyzed (Micro), or it was not tried because of scarce material (nd).

[d]For distributions with one dominant peak the position of this peak is stated with its standard deviation in parentheses. For broad distributions only the average is given. The total number of events (steps in staircases, Fig. 3) ranged between 90 and 250, in half of the mutants we performed two independent runs, only one of which is depicted in Figure 4.

[e]The cross sections are the sizes of the central dark areas of Figure 6, 100% equals 75 Å^2.

[f]Based on a model after energy minimization.

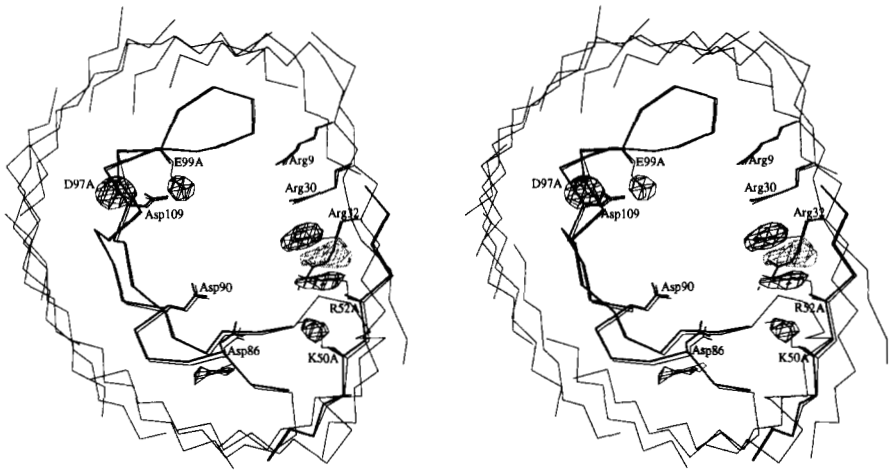

Fig. 2. Stereo view of the difference-Fourier map of the four-point mutant 50/52/97/99→A at a contour level of 3σ. Negative density is given in solid lines and positive density in dotted lines. The mutated amino acid residues are shown as part of all those forming the transversal electric field (Schulz, 1993). Part of the refined model of the mutant is depicted in thick lines, and the model of the wild-type porin in thin lines.

Del100-115 (Fig. 1). Of particular interest was the question whether loop L3 merely defines the pore size, or rather stabilizes the β-barrel and thus the whole trimer.

While L3-removal should widen the pore, a number of tryptophan mutants were designed to diminish it. Tryptophans were introduced at six positions of the eyelet, replacing Asp90, Tyr96, Glu99, Ala104, Ala116, and Ser119 (Fig. 1). The exchanges were combined in such a manner that sterical hindrance between the most abundant side-chain rotamers (Ponder & Richards, 1987) of the introduced tryptophans were avoided.

Protein production and stability

All mutants were sequenced at the DNA level. The observed mutation efficiency was around 90%. Using plasmid pET-3b-*por*, the expressed protein assembled in inclusion bodies. The expression level depended on the particular mutant. Low expression levels could not be raised by new transformation in *E. coli* BL21(DE3)pLysS or by changing the cultivation conditions including induction time. The inclusion bodies were separated and solubilized with 8 M urea. The polypeptides were folded by dilution with a detergent-containing buffer and loaded on a Q-Sepharose column. Invariably, a large fraction of the polypeptide passed this column without binding, presumably because it was not correctly folded. The bound fraction was eluted, pooled, concentrated, and dialyzed. The highest yields were around 25 mg protein per liter cell culture (Table 1).

Like many other porins, the porin from *R. blastica* migrates as a trimer in the SDS PAGE, if it has not been boiled beforehand. This applies also for the recombinant porin and also for several point mutants (Table 1). In contrast, the two L3-deletion mutants migrated as monomers, a state that usually requires boiling in SDS. This demonstrates a diminished stability of the trimeric state and thus of the whole porin. A mixture of trimers and monomers was observed for the mutant with six newly introduced tryptophans, pointing to an intermediate stability.

With most mutants we attempted to produce crystals. As many as seven mutants yielded crystals isomorphous with those of wild-type and recombinant porin and suitable for X-ray structure analysis (Table 1), demonstrating that the changes left the outer structure intact. Because crystal formation signals stability, we found that all single and double mutants as well as mutant 50/52/97/99→A remained stable, whereas the six-point mutant and both deletion mutants were labile. Lacking sufficient amounts of protein, the three-point and four-point tryptophan mutants were not screened for crystallization, although they were reasonably stable according to the SDS PAGE.

Planar lipid bilayer experiments

The porin activity of the mutants was determined in so-called reconstitution experiments using artificial planar lipid bilayer membranes (Benz & Bauer, 1988). The addition of porin to the aqueous phase resulted in a stepwise increase of the membrane conductance (Fig. 3). Each step was taken as the effect of the insertion of one porin trimer into the bilayer. Consequently, the stair cases of Figures 3A, B, and C show that the porin channels remain open after insertion. The step heights are the channel conductance values, the average of which are listed in Table 1. The mean value for the recombinant porin is the same as for the wild-type, confirming the negligible influence of mutation E1M located far away from the pore eyelet. For wild-type, recombinant, and some mutant porins, the distributions of the conductance steps (Fig. 4) were essentially unimodal with some smaller peaks at higher conductance values that presumably report simultaneous insertions of two porins.

Mutants A116K, K50A/R52A, D97A/E99A, and 50/52/97/99→A were designed to alter the charge pattern at the eyelet. They gave rise to essentially unimodal distributions, but showed higher conductance steps more frequently than the recombinant porin (Fig. 4). Here, we find that the removal of positive charges in K50A/R52A increased the conductance, whereas the removal of negative charges in D97A/E99A, as well as the addition of a positive charge in A116K, decreased it. If one assumes that positive charges at the eyelet hinder the diffusion of positive ions and vice versa, these observations fit the known ion selectivity of the

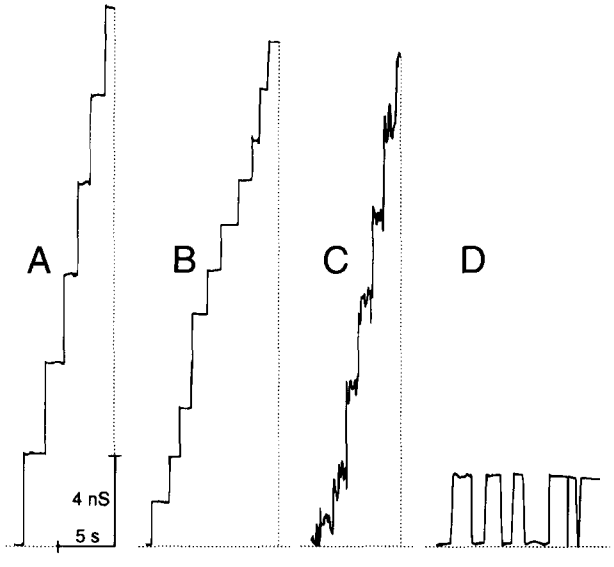

Fig. 3. Ionic currents representing conductances through planar lipid bilayers formed by diphytanoylphosphatidylcholine dissolved in *n*-decane. The steps record the insertion of single molecules of purified C_8E_4-solubilized trimeric porins from *R. blastica* using Triton X-100 as an additive. The conductance scale and the time scale can be derived from the respective bars given in A. (**A**) Recombinant porin; (**B**) mutant 99/116→W; (**C**) mutant Del100–115; (**D**) mutant 90/96/99/104/116/119→W at concentrations below 10 ng/mL.

wild-type porin (Butz et al., 1993), which showed a much higher permeation rate for cations than for anions (13 times for KCl) and, thus, a predominance of the effects on cations.

In detail, the four mutants K50A/R52A, 50/52/97/99→A, A116K, and D97A/E99A change the net charge at the eyelet by −2, 0, +1, and +2, respectively. The corresponding conductances are 4.2, 3.9, 3.2, and 3.7 nS (Table 1) showing a dependence in the expected direction. Mutant A116K shows an especially low conductance that is most likely caused by the concomitant reduction of the eyelet cross section (see below). Because the charge effects are rather small, we conclude that the transversal electric field is not crucial for ion permeation.

With the L3 deletion and the tryptophan mutants, we intended to change the eyelet size. Both deletion mutants failed to widen the pore, however, because the conductance steps were generally smaller than those of the wild-type (Fig. 4). Moreover, the conductance curve was noisy (Fig. 3C). The noise is most likely caused by structural fluctuations of the inserted pores, i.e., instability, in correspondence with the low production rates and SDS PAGE migration (Table 1). We, therefore, conclude that the constriction loop L3 is essential for maintaining the structure of the 16-stranded β-barrel, as suggested early on by its rigidity (Weiss & Schulz, 1992). Our conclusion contradicts molecular dynamics calculations (Soares et al., 1995) and also Van Gelder et al. (1997), who proposed that L3 is mobile and that this is of functional importance. In agreement with our observations, the L3-deletion mutants selected by growth on large nutrients like maltodextrins are also rather labile (Rocque & McGroarty, 1990; Lou et al., 1996; Saint et al., 1996a).

Narrowing the eyelet by introducing bulky tryptophans gave rise to a variety of behaviors in the lipid bilayer experiments (Fig. 4). The single mutant 104→W and the two double mutants 96/119→W and 99/116→W showed dominant peaks with maxima shifted to lower conductance values in agreement with pore nar-

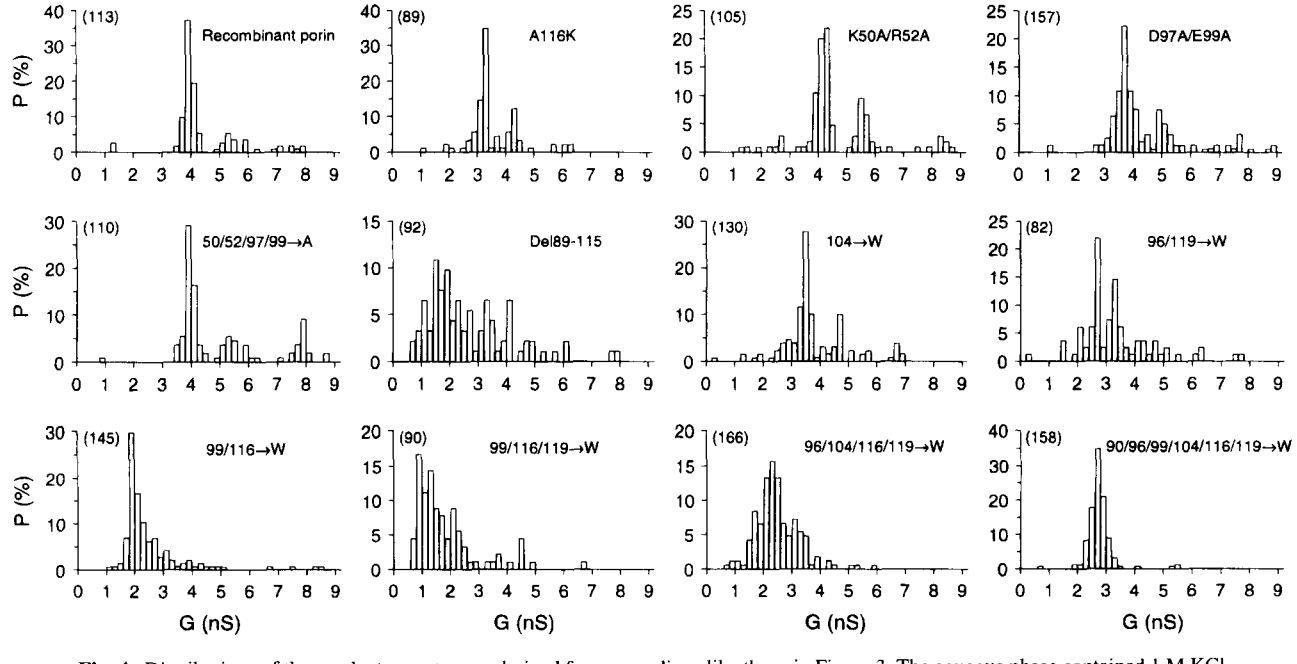

Fig. 4. Distributions of the conductance steps as derived from recordings like those in Figure 3. The aqueous phase contained 1 M KCl on both sides of the membrane, the porins were added to both sides, the voltage was 20 mV. The respective mutants are indicated. The conductance steps G are in nS, the total number of steps in the run is given in parentheses, P is the percentage of events in one of the bins. Not shown are the distributions of wild type, Del100-115, and 90/99/116→W, which resemble those of the depicted recombinant porin, Del89-115, and 99/116/119→W, respectively.

rowing. Moreover, there was not much noise in the conductance curves (Fig. 3B). When introducing more tryptophans like in the three-point and four-point mutants, the porins became more labile, as demonstrated by the rather low production rates (Table 1), by the noisy conductance curves, and by the broad distribution of conductance step sizes (Fig. 4).

The behavior of the six-point mutant 90/96/99/104/116/119→W differed drastically from those of the others (Fig. 3D). In contrast to all other mutants, the conductance steps did not add up, but broke down after about 2 s. Furthermore, the conductance curve is not noisy. This mutant is labile because it can only be produced in small amounts and because it is partially monomerized in SDS PAGE. We suggest that this porin collapses shortly after incorporation into the membrane and closes its channel, presumably as a consequence of the applied voltage across the pore (20 mV). Such a voltage closure is known for mitochondrial porins, which also showed a resembling conductance curve with short-lived single events (Benz, 1994). Furthermore, closures are known for bacterial porins at voltages around 150 mV (Jeanteur et al., 1994). For mutants, the closure voltages are often lowered, most likely because of decreased stability (Bishop et al., 1996; Gokce et al., 1997).

X-ray structure analysis

The crystals of the porin mutants diffracted to resolutions around 2 Å like those obtained from wild-type and recombinant porins (Kreusch & Schulz, 1994; Schmid et al., 1996). X-ray data were collected for seven mutants (Table 2). Initial $(F_{mut,obs} - F_{wt,calc})$ $\exp(i\alpha_{wt,calc})$ difference-Fourier maps contained only a few regions with density. These were interpreted and the resulting structures were refined (Table 2). One of the changes confirmed mutation E1M of the recombinant porin, which is ignored in the mutant names. The other density differences concerned the exchanges to lysine, to alanines, or to tryptophans at the eyelet. In the four-point mutant 50/52/97/99→A, the expected negative peaks around the deleted side chains were accompanied by positive density close to the side chain of Arg32, indicating its displacement (Fig. 2). Actually, the guanidinium group of Arg32 moved toward the position formerly occupied by the guanidinium group of Arg52 and became more mobile: its *B*-factor increased from 13 to 30 Å^2.

All changes observed in mutant 50/52/97/99→A turned out to be present either in mutant K50A/R52A, like the displacement of Arg32, or in mutant D97A/E99A. Obviously, the mutational effects added up linearly, presumably as a consequence of K50 with R52 being at one side of the pore eyelet and D97 with E99 at the other (Figs. 1, 2). In mutant A116K, the side chain of the introduced lysine is completely embedded in density and assumes a well-defined conformation extending into the lumen of the eyelet, which causes an appreciable reduction of the cross section (Table 1).

The structure of mutant 104→W (Fig. 5A) revealed that the introduced tryptophan adopted an unusual rotamer, placing the indole along the barrel wall, which gave rise to a mere 4% reduction of the eyelet cross section (Fig. 6A,C). When both Tyr96 and Ser119 were replaced by tryptophan (Fig. 5B), the cross section of the pore was reduced to 78% of that of the wild type (Fig. 6D). In contrast, the double mutant 99/116→W decreased the pore size to merely 45% of that of the wild type (Fig. 6E). Here, Trp116 replaced an alanine and pointed into the lumen of the eyelet, whereas Trp99 replacing a glutamate remained at its rim (Fig. 5C).

The structure of the six-point mutant was modeled under the assumption that the mutations can be superimposed. Accordingly, tryptophans 96, 99, 104, 116, and 119 were built using the conformations observed in the structurally established mutants, and

Table 2. *X-ray data collection and structural refinement of the porin mutant crystals*

	A116K	K50A/R52A	D97A/E99A	50/52/97/99→A	104→W	96/119→W	99/116→W
Resolution range (Å)	20–2.19	20–2.04	33–2.25	26–2.30	13–1.90	12–2.00	33–1.93
Last shell (Å)	2.31–2.19	2.15–2.04	2.37–2.25	2.38–2.30	1.97–1.90	2.07–2.00	2.00–1.93
Unique reflections[a]	25,831(3,665)	32,040(4,676)	23,941(3,524)	20,686(1,565)	34,853(2,094)	32,123(2,657)	31,332(1,895)
Redundancy[a]	3.7(3.5)	3.5(2.2)	3.7(3.7)	2.9(1.4)	2.5(1.3)	2.2(1.4)	2.4(1.3)
R_{sym} (%)[a,b]	5.6(22.3)	4.5(18.1)	4.4(13.2)	6.5(18.5)	3.8(19.0)	4.6(14.2)	3.9(18.9)
Completeness (%)[a]	99(95)	100(100)	100(100)	93(72)	86(51)	92(78)	82(52)
R-factor (%)[c]	15.3	16.3	21.5	17.7	17.0	16.3	18.5
Free *R*-factor (%)[d]	18.1	18.6	25.1	21.5	19.0	18.8	20.5
Number of atoms[e]	2,178/142/63	2,167/178/42	2,156/61/21	2,149/98/63	2,201/116/63[f]	2,227/136/63	2,193/107/63[f]
B-factors (Å^2)[e]	31/39/78	32/49/79	30/28/62	31/39/76	30/36/80[f]	26/33/77	29/34/71[f]
RMSD main chain (Å)[g]	0.18	0.18	0.21	0.24	0.15	0.17	0.20

[a]All values in parentheses refer to the last shell.

[b]$R_{sym} = \sum_{h,i} |I(h)_i - \langle I(h)\rangle| \Big/ \sum_{h,i} I(h)_i$.

[c]The RMSD bond length and bond angles ranges were 0.013–0.022 Å and 2.2–2.8°, respectively.

[d]The size of the separated set ranged always around 10%.

[e]The values are for protein/water/detergent C_8E_4. The *B*-factors are averages. In all cases there were no significant main-chain *B*-factor changes at the mutations.

[f]In these refinements there is a putative Mg^{2+} ion between Ser28 and Asp57 at the inner barrel wall 9 Å away from the eyelet toward the periplasm. It shows a *B*-factor of around 45 Å^2.

[g]The deviations are between the respective mutant and the wild-type for all main-chain atoms. The RMSD for all protein atoms range between 0.5 and 0.6 Å.

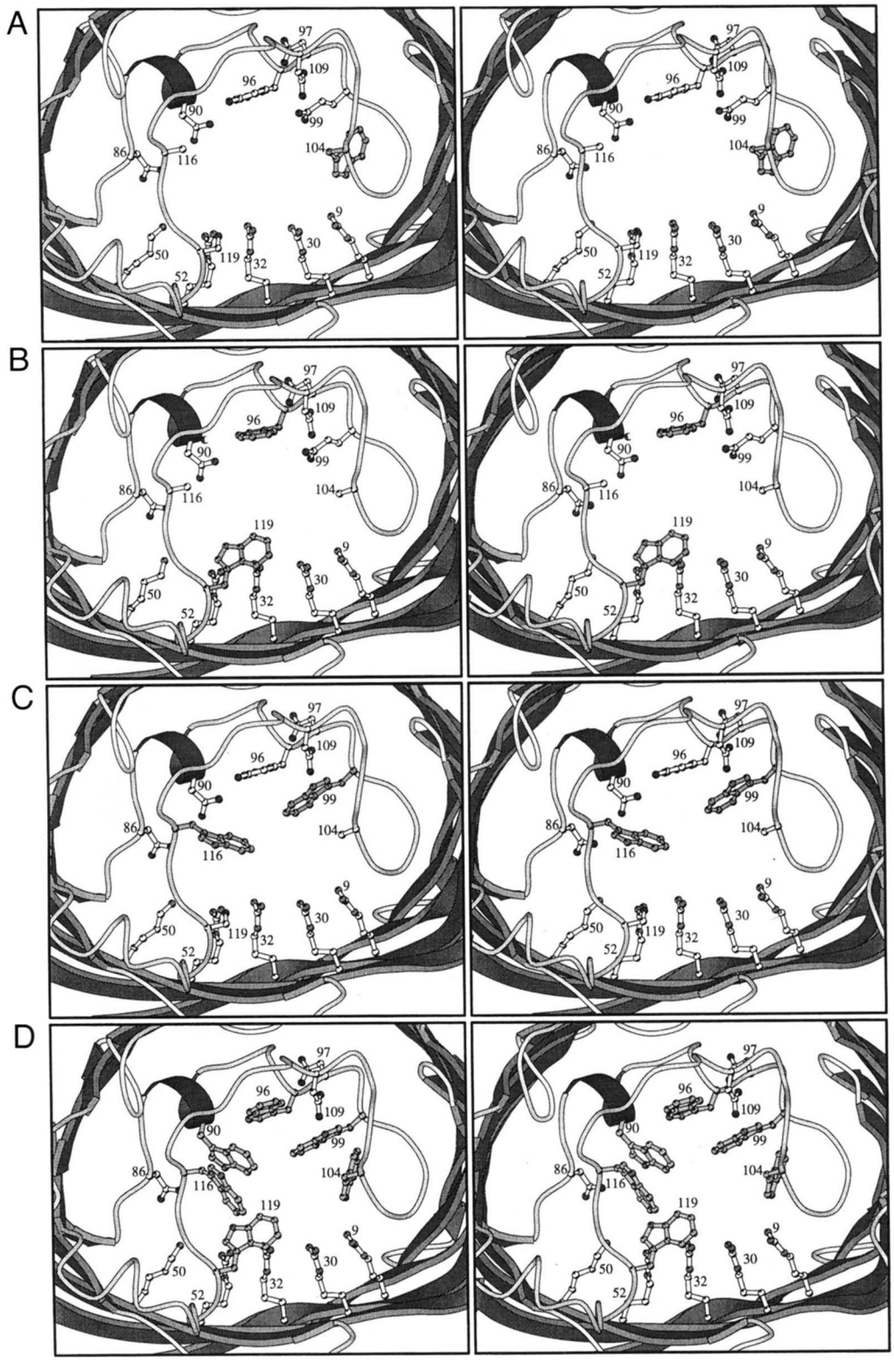

Fig. 5. Structures of several tryptophan mutants. All stereoviews are from the external medium into the pore eyelet exactly along the molecular threefold axis. (**A**) Refined structure of mutant 104→W; (**B**) refined structure of mutant 96/119→W; (**C**) refined structure of mutant 99/116→W; (**D**) model of mutant 90/96/99/104/116/119→W as described in the text.

Trp90 was introduced using the most frequent rotamer (Ponder & Richards, 1987). To avoid steric hindrance, all six modeled tryptophan side chains were relaxed by an energy minimization run in X-PLOR (Brünger, 1993). The resulting model is shown in Figure 5D. Compared with the wild-type, its eyelet cross section is reduced to a mere 22% (Fig. 6F).

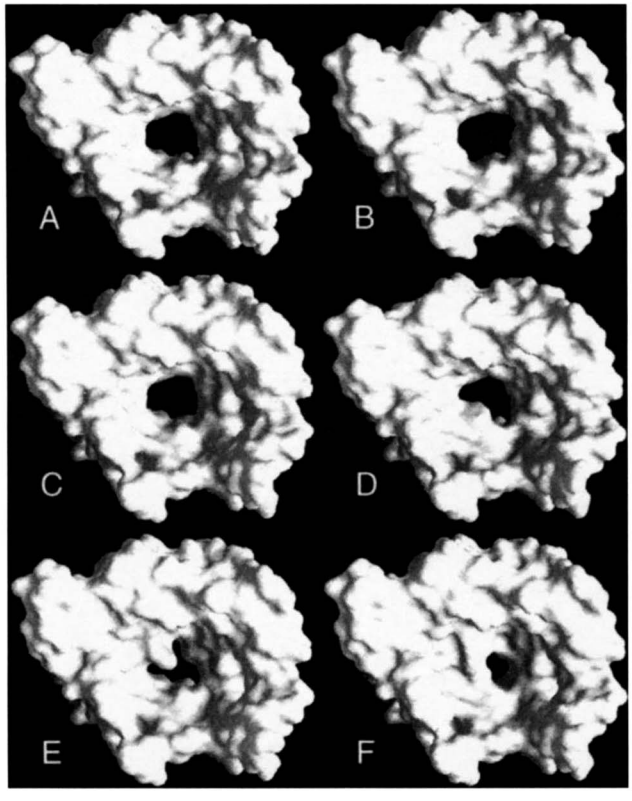

Fig. 6. Molecular surfaces calculated with the program GRASP (Nicholls et al., 1991). The view is exactly along the threefold axis from the external medium. The open cross-section areas of the eyelets are given in Table 1. (**A**) Recombinant porin from *R. blastica* with a cross section of 75 Å^2; (**B**) mutant 50/52/97/99→A, (**C**) mutant 104→W; (**D**) mutant 96/119→W; (**E**) mutant 99/116→W; (**F**) model of mutant 90/96/99/104/116/119→W.

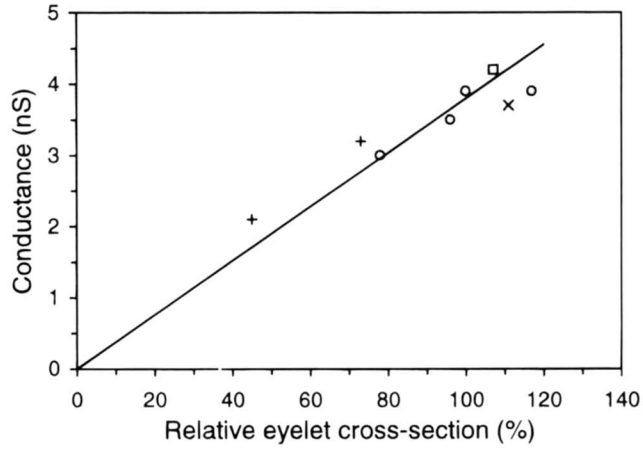

Fig. 7. Relationship between conductance and relative cross section as listed in Table 1. The symbols report the net charge difference (delta) introduced by the mutations: delta = −2 for K50A/R52A (open squares), delta = 0 for recombinant, 50/52/97/99→A, 104→W, and 96/119→W (open circles), delta = +1 for A116K and 99/116→W (+), delta = +2 for D97A/E99A (×). The regression line going through the origin is given.

Correlation between conductance, cross section, and charge pattern

The X-ray analyses showed an additivity of the structural changes of mutants K50A/R52A and D97A/E99A to yield those of mutant 50/52/97/99→A. Accordingly, the corresponding eyelet cross sections 107 and 111% add up to 118%, which is close to the observed 117% of the four-point mutant. The same applies for the conductances, where the respective values of 4.2 and 3.7 nS average out to 3.95 nS, which is near the observed 3.9 nS. We conclude that not only the structures but also the conductances of these spatially separated mutations show additivity.

If we plot the conductance as a function of the cross section, we observe an approximately linear dependence over a broad range (Fig. 7). This confirms rather directly that the channel conductances follow the usual electricity laws. Interestingly enough, this distribution demonstrates that the charge pattern at the eyelet is of minor importance for ion conductivity because all mutants, including those with charge modifications, lie near the regression line.

Still, an effect can be discerned if only the three charge-modifying mutants with minor cross-sectional changes, namely D97A/E99A, 50/52/97/99→A, and K50A/R52A, are considered. Indeed, their relative conductances (95, 100, and 108%) follow the net charge changes (+2, 0, −2) at the eyelet, in agreement with the known cation selectivity (Butz et al., 1993). Mutants A116K and 99/116→W do not follow this rule. Both showed an appreciable reduction of the cross section, the effect of which is likely to conceal the smallish contribution from the +1 net charge change. The minor role of charge effects for ionic conductance does not contradict the suggested importance of the transversal electric field across the eyelet, because this field is required for discrimination against nonpolar solutes (Schulz, 1993).

The conductance of the six-point mutant was 69% of that of the wild type, which was much larger than to be expected from its putative cross section of 22% (Table 1, Fig. 7). Therefore, the structural model (Figs. 5D, 6F) does not correlate with the lipid bilayer experiments. The stability parameters of Table 1 demonstrate that this mutant is labile, and thus contradict the reproducibility of the short-lived conductance events, the absence of noise (Fig. 3D), and the unimodal distribution (Fig. 4). We propose that this porin assumes two states, one of which has a much larger eyelet than expected from Figure 6F, and the other has a closed pore.

Conclusions

The elucidation of membrane channel structures allowed for rational engineering on them. Most work was done with the porins, but also other pores like α-haemolysin have been modified (Braha et al., 1997). As for porins, the structures and the growth-selected mutants showed the importance of the constriction loop L3. The proposal that L3 is mobile and that this mobility is essential for the function (Soares et al., 1995; Van Gelder et al., 1997), however, is not supported by our data because L3 has low *B*-factors in all structures presented here, as in similar porins (Weiss & Schulz, 1992). L3 is tightly attached to the inner barrel wall, and the introduced deletions in this loop clearly rendered the whole porin labile (Table 1).

Our mutation series demonstrated that the ion conductance correlates with the eyelet cross section, if the labile deletion mutants with their noisy conductance curves and generally smallish steps are excluded. The effect of charge alterations at the eyelet on the ion conductances are only of a minor nature. The isomorphous

crystals of seven mutants confirm that pore engineering means modifying a cavity that is surrounded by a stable shell and, therefore, more amenable for a structure analysis. Conceivably, such a cavity engineering could provide useful data on the stabilities of peptides.

Because porins are rather stable and to some extent selective, it appears possible to incorporate them into sturdy synthetic membranes and use these as filters. For such purposes the constricting eyelet could be engineered to change selectivities. Here, we began with such endeavors by changing the charge pattern and the cross section.

Materials and methods

Mutagenesis, protein expression, and purification

The expression plasmid pET-3b-*por* had been constructed as described (Schmid et al., 1996). For site-directed mutagenesis the gene was taken out with *Xba*I and *Bam*HI and cloned into bacteriophage vector M13mp19 (Boehringer-Mannheim, Germany). The mutations were performed with the phosphorothioate method of Taylor et al. (1985) using a kit from Amersham, Germany. DNA was sequenced with a direct blotter (GATC-1500) using the BioCycle Sequencing Kit (GATC) with Thermo Sequenase from Amersham.

The mutants were expressed in inclusion bodies within *E. coli* strain BL21(DE3)pLysS and (re)natured and purified as described for the recombinant porin (Schmid et al., 1996). The mutants were analyzed by SDS PAGE (boiled for 5 min as well as unboiled). The protein concentrations were determined photometrically (Gill & von Hippel, 1989).

Planar lipid bilayer experiments

The applied method has been described by Benz & Bauer (1988). The hole diameter of the Teflon divider was 0.8 mm. The membrane was formed by "painting" a 1% (w/v) solution of diphytanoylphosphatidylcholine (Avanti Polar-Lipids, Alabama) in *n*-decane over the hole. For all experiments 1 M KCl was the electrolyte on both sides of the membrane, and the temperature was kept at 25 °C. The total volume of both cells was 10 mL. The porin was added to both sides as a solution of about 2–10 mg/mL protein in 20 mM Tris/HCl at pH 7.2, 300 mM LiCl, 0.6% (w/v) *n*-octyltetraoxyethylene (C_8E_4) together with Triton X-100. Triton stimulated the insertions as described by De Cock et al. (1996), but caused no steps on its own. No conductance steps were detectable without Triton. The final amount of porin in the cells ranged between 1–40 μg. Interestingly enough, the amount of the six-point mutant had to remain below 0.1 μg for obtaining the single steps shown in Figure 3D.

Crystallization and structure analysis

The crystallization procedure followed Kreusch et al. (1994). Crystals appeared after one to two weeks and grew within one to two months to sizes of about (500 μm)^3. They all belonged to space group R3 with cell parameters within ±1% equal to those of the wild-type crystals ($a_{hex} = b_{hex} = 104.3$ Å, $c_{hex} = 124.6$ Å). Data were collected on a rotating anode X-ray generator with an area detector, either model RU200B (Rigaku) with model X1000 (Siemens) or model RU2HC (Rigaku) with a 30-cm imaging plate (MARresearch). The data were processed with program XDS (Kabsch, 1988) and with program MOSFLM (Leslie, 1987), respectively. After a first round of rigid-body refinement, the appropriate changes were introduced in the models, according to the respective difference-Fourier maps. The resulting models were further refined using program REFMAC (Murshudov et al., 1997). Water molecules were automatically introduced/removed and refined using a procedure that alternates between program REFMAC and ARP (Lamzin & Wilson, 1993). The stereo figures were produced with program MOLSCRIPT (Kraulis, 1991). All coordinates and structure factors are deposited in the Protein Data Bank under accession code 2PRN, 3PRN, 5PRN, 6PRN, 7PRN, 8PRN, 1BH3.

Acknowledgments

We thank Prof. Dr. J. Weckesser for help with the conductance measurements. The project was supported by the Deutsche Forschungsgemeinschaft under Sfb-60, and by a grant from the Association Française pour la Recherche Thérapeutique (L.M.).

References

Bauer K, Struyvé M, Bosch D, Benz R, Tommassen J. 1989. One single lysine residue is responsible for the special interaction between polyphosphate and the outer membrane porin PhoE of *Escherichia coli*. *J Biol Chem 264*:16393–16398.

Benson SA, Occi JLL, Sampson BA. 1988. Mutations that alter the pore function of the OmpF porin of *Escherichia coli* K12. *J Mol Biol 203*:961–970.

Benz R. 1994. Permeation of hydrophilic solutes through mitochondrial outer membranes: Review on mitochondrial porins. *Biochim Biophys Acta 1197*: 167–196.

Benz R, Bauer K. 1988. Permeation of hydrophilic molecules through the outer membrane of Gram-negative bacteria. *Eur J Biochem 176*:1–19.

Bishop ND, Lea EJA, Mobasheri H, Spiro S. 1996. Altered voltage sensitivity of mutant OmpC porin channels. *FEBS Lett 379*:295–298.

Braha O, Walker B, Cheley S, Kasianowicz JJ, Song L, Gouaux JE, Bayley H. 1997. Designed protein pores as components for biosensors. *Chem Biol 4*:497–505.

Brünger AT. 1993. *X-PLOR version 3.1: A system for X-ray crystallography and NMR*. New Haven, CT: Yale University Press.

Butz S, Benz R, Wacker T, Welte W, Lustig A, Plapp R, Weckesser J. 1993. Biochemical characterization and crystallization of porin from *Rhodopseudomonas blastica*. *Arch Microbiol 159*:301–307.

De Cock H, van Blokland S, Tommassen J. 1996. *In vitro* insertion and assembly of outer membrane protein PhoE of *Escherichia coli* K-12 into the outer membrane. Role of Triton-X-100. *J Biol Chem 271*:12885–12890.

Gill SC, von Hippel PH. 1989. Calculation of protein extinction coefficients from amino acid sequence data. *Anal Biochem 182*:319–326.

Gokce I, Bainbridge G, Lakey JH. 1997. Stabilising and destabilising modifications of cysteines in the *E. coli* outer membrane porin protein OmpC. *FEBS Lett 411*:201–205.

Jeanteur D, Schirmer T, Fourel D, Simonet V, Rummel G, Widmer C, Rosenbusch JP, Pattus F, Pagès J-M. 1994. Structural and functional alterations of a colicin-resistant mutant of OmpF porin from *Escherichia coli*. *Proc Natl Acad Sci USA 91*:10675–10679.

Kabsch W. 1988. Evaluation of single-crystal X-ray diffraction data from a position-sensitive detector. *J Appl Crystallogr 21*:916–924.

Kraulis PJ. 1991. MOLSCRIPT: A program to produce both detailed and schematic plots of protein structures. *J Appl Crystallogr 24*:946–950.

Kreusch A, Neubüser A, Schiltz E, Weckesser J, Schulz GE. 1994. Structure of the membrane channel porin from *Rhodopseudomonas blastica* at 2.0 Å resolution. *Protein Sci 3*:58–63.

Kreusch A, Schulz GE. 1994. Refined structure of the porin from *Rhodopseudomonas blastica*. Comparison with the porin from *Rhodobacter capsulatus*. *J Mol Biol 243*:891–905.

Lamzin VS, Wilson KS. 1993. Automated refinement of protein models. *Acta Crystallogr D49*:129–147.

Le Dain AC, Häse CC, Tommassen J, Martinac B. 1996. Porins of *Escherichia coli*: Unidirectional gating by pressure. *EMBO J 15*:3524–3528.

Leslie AGW. 1987. Profile fitting. In: Helliwell JR, Machin PA, Papiz MZ, eds. *Computational aspects of protein crystal data analysis. Proceedings of the Daresbury study weekend*. Warrington, UK: Daresbury Laboratory. pp 39–50.

Lou KL, Saint N, Prilipov A, Rummel G, Benson SA, Rosenbusch JP, Schirmer T. 1996. Structural and functional characterization of OmpF porin mutants selected for larger pore size. I. Crystallographic analysis. *J Biol Chem 271*:20669–20675.

Misra R, Benson SA. 1988. Isolation and characterization of OmpC porin mutants with altered pore properties. *J Bacteriol 170*:528–533.

Murshudov GN, Vagin AA, Dodson EJ. 1997. Refinement of macromolecular structures by the maximum-likelihood method. *Acta Crystallogr D53*:240–255.

Nicholls A, Sharp KA, Honig B. 1991. Protein folding and association: Insights from the interfacial and thermodynamic properties of hydrocarbons. *Proteins Struct Funct Genet 11*:281–296.

Nikaido H. 1994. Porins and specific diffusion channels in bacterial outer membranes. *J Biol Chem 269*:3905–3908.

Ponder JW, Richards FM. 1987. Tertiary templates for proteins. Use of packing criteria in the enumeration of allowed sequences for different structural classes. *J Mol Biol 193*:775–791.

Przybylski M, Glocker MO, Nestel U, Schnaible V, Blüggel M, Diederichs K, Weckesser J, Schad M, Schmid A, Welte W, Benz R. 1996. X-ray crystallographic and mass spectrometric structure determination and functional characterization of succinylated porin from *Rhodobacter capsulatus*: Implications for ion selectivity and single-channel conductance. *Protein Sci 5*:1477–1489.

Rocque WJ, McGroarty EJ. 1990. Structure and function of an OmpC deletion mutant porin from *Escherichia coli* K-12. *Biochemistry 29*:5344–5351.

Saint N, Lou KL, Widmer C, Luckey M, Schirmer T, Rosenbusch JP. 1996a. Structural and functional characterization of OmpF porin mutants selected for larger pore size. II. Functional characterization. *J Biol Chem 271*:20676–20680.

Saint N, Prilipov A, Hardmeyer A, Lou KL, Schirmer T, Rosenbusch JP. 1996b. Replacement of the sole histidinyl residue in OmpF porin from *E. coli* by threonine (H21T) does not affect channel structure and function. *Biochem Biophys Res Commun 223*:118–122.

Schmid B, Krömer M, Schulz GE. 1996. Expression of porin from *Rhodopseudomonas blastica* in *Escherichia coli* inclusion bodies and folding into exact native structure. *FEBS Lett 381*:111–114.

Schulz GE. 1993. Bacterial porins: Structure and function. *Curr Opin Cell Biol 5*:701–707.

Schulz GE. 1996. Porins: General to specific, native to engineered passive pores. *Curr Opin Struct Biol 6*:485–490.

Soares CM, Björkstén J, Tapia O. 1995. L3 loop-mediated mechanisms of pore closing in porin: A molecular dynamics perturbation approach. *Protein Eng 8*:5–12.

Srikumar R, Dahan D, Arhin FF, Tawa P, Diederichs K, Coulton JW. 1997. Porins of *Haemophilus influenzae* type b mutated in loop 3 and in loop 4. *J Biol Chem 272*:13614–13621.

Taylor JW, Ott J, Eckstein F. 1985. The rapid generation of oligonucleotide-directed mutations at high frequency using phosphorothioate-modified DNA. *Nucleic Acids Res 13*:8765–8785.

Van Gelder P, Saint N, van Boxtel R, Rosenbusch JP, Tommassen J. 1997. Pore functioning of outer membrane protein PhoE of *Escherichia coli*: Mutagenesis of the constriction loop L3. *Protein Eng 10*:699–706.

Weiss MS, Schulz GE. 1992. Structure of porin refined at 1.8 Å resolution. *J Mol Biol 227*:493–509.

Weiss MS, Wacker T, Weckesser J, Welte W, Schulz GE. 1990. The three-dimensional structure of porin from *Rhodobacter capsulatus* at 3 Å resolution. *FEBS Lett 267*:268–272.